Title

Stationary-Mixing Field-Programmable Pin-Constrained Digital Microfluidic Biochip

Permalink

https://escholarship.org/uc/item/9rg877j1

Authors

Abdoli, Alireza
Brisk, Philip

Publication Date

2018-07-01

DOI

10.1016/j.mejo.2018.05.005

Peer reviewed

Stationary-Mixing Field-Programmable Pin-Constrained Digital Microfluidic Biochip

Alireza Abdoli, Philip Brisk [*]

Department of Computer Science and Engineering, University of California, Riverside, USA

ABSTRACT

This paper introduces a Field Programmable Pin-Constrained (FPPC) architecture for a Digital Microfluidic Biochip (DMFB) that integrates a new stationary hydrodynamic mixing technology. Compared to the traditional rotation-based mixing, stationary mixing is faster, requires fewer electrodes, and limits residue production and the likelihood of biofouling. Although the stationary mixing principle has been established, programmable DMFB architectures that feature stationary mixing have not been investigated or evaluated. Simulation results show that the Stationary Mixing FPPC (SM-FPPC) architecture introduced here outperforms existing Direct Addressing (DA) and FPPC DMFBs that employ traditional rotation-based mixing. An analysis based on a commercially available Printed Circuit Board (PCB) cost calculator demonstrates a 31% reduction in cost compared to the lowest cost PCB reported in prior literature.

1. Introduction

Laboratory-on-a-chip (LoC) technology integrates one or more benchtop-scale laboratory procedures into a single micro-scale chip, reducing both time and cost through miniaturization and automation. Among the competing LoC technologies, Digital Microfluidic Biochips (DMFBs) [1–6], based on the principle of electrowetting [7], offer the additional benefits of programmability and scalable low-cost fabrication based on traditional Printed Circuit Board (PCB) manufacturing technology. Successful DMFB demonstrations have been reported for biochemical applications including DNA amplification [8], air/water pollution monitoring [9], analysis of bacterial resistance to antibiotics [10], epigenetics [11], cellular genetic engineering [12], and wine tasting [13], among many others. As a result, there is great interest in developing techniques to improve the performance and reduce the cost of DMFBs in practice.

Fluid transport and mixing are two of the most fundamental capabilities that virtually all LoCs are capable of performing. Historically, DMFBs perform mixing by merging two liquid droplets (via transport) and then physically moving the merged droplet back and forth [1], which is effectively a transport operation, although often restricted to a relatively small sub-region of the device. One of the drawbacks of rotation-based mixing—which has historically lacked an alternative short of switching to another LoC technology—is that certain biological samples, such as proteins, have a tendency to absorb onto the chip surface; as a result, repeated transport of droplets containing such samples

leads to biofouling, cross-contamination, and, eventually, physical degradation of the underlying substrate [14].

Recently, stationary hydrodynamic mixing has been introduced as an alternative to rotation-based mixing [14]. The basic principle is to hold a droplet in place and to generate flow circulation by applying a high frequency AC voltage to the droplet. This induces internal circulation within the droplet, leading to faster mixing times than traditional rotation-based mixing, and eliminates the drawbacks listed above. The impact of stationary mixing on bioassay execution time has not yet been quantified, either through experimentation or simulation. Likewise, fully integrated DMFB architectures that perform stationary mixing have not yet been proposed or evaluated.

In response, this paper introduces a Stationary Mixing Field-Programmable Pin-Constrained (SM-FPPC) DMFB and its compiler. The compilation process is similar to that of an earlier FPPC DMFB design that features rotation-based mixing [15], but includes a few subtle differences. We estimate the cost of Printed Circuit Boards (PCBs) for two SM-FPPC variants, and show that the cheaper variant costs 31% less than the lowest cost PCB for a traditional FPPC DMFB. Through simulation, we show than the SM-FPPC runs faster than both Direct Addressing and FPPC DMFBs of comparable size, due to faster mixing times and slightly shorter droplet routes. As stationary mixing can be accomplished using a 1×3 electrode configuration, more and faster concurrent mixing operations can be performed on a fixed-size device when compared to traditional rotation-based mixing.

---

* Corresponding author.
  E-mail address: philip@cs.ucr.edu (P. Brisk).

2. Background

The basic principle underlying digital microfluidics is the electro-wetting effect [7], depicted below in Fig. 1: applying a voltage to a droplet changes its shape: the contact angle with the surface flattens, and a greater portion of the droplet comes into contact with the surface, effectively "wetting" it.

As shown in Fig. 2(a), a DMFB is a 2D array of patterned electrodes separated from fluid by an insulating hydrophobic layer [1–6]. In Fig. 2(b) An optional top plate may contain a ground electrode, which can assist with droplet movement. Droplets in the system must be slightly wider than an electrode in order to induce movement.

Fig. 3 depicts the basic principles underlying droplet movement in a DMFB. Activating control electrode CE2 underneath the droplet holds it in place (left). It is important to observe that the droplet length is greater than the length of CE2, and it extends into the physical space above control electrodes CE1 and CE3 as well. Activating CE3 in addition to CE2 creates a horizontal force that centers the droplet between the two electrodes (middle); this force can only be induced because a portion of the droplet in its initial position is directly on top of CE3. Lastly, deactivating CE2, while leaving CE3 activated, releases the portion of the force that hold the droplet between CE2 and CE3, allowing the droplet to fully position itself on top of CE3 (right).

Droplet motion induced by electrode activation and deactivation provides a DMFB with an instruction set architecture (ISA) containing five instructions, as shown in Fig. 4: Transport, Split, Merge, Mix, Store. As the DMFB itself is a spatially parallel array consisting of a uniform set of electrodes, each of these operations can be performed anywhere on the surface of the chip; thus, the DMFB is "reconfigurable" [16].

In addition to the five reconfigurable operations, a DMFB typically supports several non-reconfigurable operations as well. For example, input and output (including waste production) use reservoirs that are physically placed on the perimeter of the chip; the locations and roles of the reservoirs do not change when the DMFB is in use, so they are not reconfigurable. External devices such as sensors, mixers, and heaters may be placed at any location on the chip surface [17–31]; such locations can still perform the five basic operations, but are now enhanced with additional capabilities. Similarly, specialized electrodes can be fabricated to perform operations such as electroporation [12] or non-uniform splitting [32].

3. Rotation-based and stationary mixing

Historically, DMFBs have performed mixing by sectioning off a rectangular sub-array of the chip (1×4, 2×2, etc.); we refer to these as rotation-based mixers. Prior work has shown that the size of the sub-array and the path that the droplet travels through the sub-array impact mixing time [15]. In general, larger mixers yield shorter mixing time, but consume more spatial on-chip area, thereby reducing the amount of available parallelism; this creates a tradeoff that must be properly evaluated when determining how to best map a bioassay onto a DMFB for high-throughput execution [33–35].

Recently, stationary mixing, in which an AC activation voltage is applied to an otherwise stationary droplet, has emerged as an alternative to rotation-based mixing [14]. If the voltage is applied by inserting a wire directly into the droplet, as shown in Fig. 5(a), the regions with the

highest intensity electric fields heat up, resulting in a temperature gradient that alters the permittivity and conductivity of the droplet, inducing a gradient of properties throughout the droplet. This, in turn, creates an electrohydrodynamic effect that generates circulating motion; in general, liquids with higher conductivity require higher frequencies to induce this effect.

A slightly different approach is required to induce stationary mixing using a DMFB, i.e., 2D array of patterned electrodes, which does not include a mechanism to insert a wire directly into the droplet. To induce stationary mixing in a DMFB, as shown in Fig. 5(b), adjacent $1.5 \, mm \times 1.5 \, mm$ electrodes separated by $\sim 30 \, \mu m$ are actuated with applied voltages of opposite polarities. In Fig. 5(c) and (d), the same principle can be applied to a DMFB that features a closed top plate with a single electrode; activating the top plate in conjunction with the patterned electrodes at the bottom generates a stronger electric field gradient within the droplet, leading to faster mixing.

Stationary mixers offer faster mixing times that traditional rotation-based mixers while consuming less on-chip area. Ref. [15] reported a $\sim 10 \, s$ mixing time for a 2×2 rotation-based mixer, compared to $\sim 6 \, s$ for a 3×2 rotation-based mixer and $\sim 3 \, s$ for a 4×2 rotation-based mixer. In contrast, Ref. [14] reports stationary mixing times of less than 1 s, depending on the AC voltage applied and the actuation frequency.

The performance of stationary mixing depends on several parameters, which Ref. [14] discussed in great detail. In general, increasing the frequency and/or amplitude of the applied AC voltage reduced the mixing time, up to a threshold; beyond the threshold, the droplet undergoing stationary mixing shed pico-liter "satellite" droplets, thereby reducing volume (and potentially contaminating other droplets nearby). Mixing efficiency was shown to improve when the gap between top and bottom plates increased, with benefits saturating at $\sim 350 \, \mu m$. The introduction of salts and DNA to the samples decreased electrothermal effects, which could be compensated by increasing the frequency of the applied AC voltage; using a thermal imaging camera, it was shown that doing this induced a negligible increase in droplet temperature. Typical operating parameters based on the experiments reported in Ref. [14] were to apply a 100 V root-mean-squared (RMS) AC voltage at 1 kHz using a sine waveform.

4. Stationary Mixing Field-Programmable Pin-Constrained DMFB

This section desires a low-cost programmable DMFB architecture that can integrate stationary mixing; here, we restrict our discussion to standard electronic Printed Circuit Board (PCB) fabrication. Prior work has shown that the foremost cost-drivers for PCB-based DMFBs are the number of PCB layers, followed by the number of control pins [36]. The most expensive DMFBs are typically those that employ direct addressing, i.e., each control pin drives exactly one electrode; the number of PCB layers is determined by an escape route, which connects each internal electrode to a control pin on the perimeter of the chip [37,38]. The quality of the escape routing algorithm can significantly impact the number of PCB layers required.

Pin-sharing [39] allows one control pin to drive several electrodes, which reduces the total number of signals that must be delivered to the PCB, thereby reducing cost. Overly aggressive pin-sharing can be detrimental to PCB escape routing when a single wire must connect electrodes across the entire 2D span of the chip, creating blockages that push other
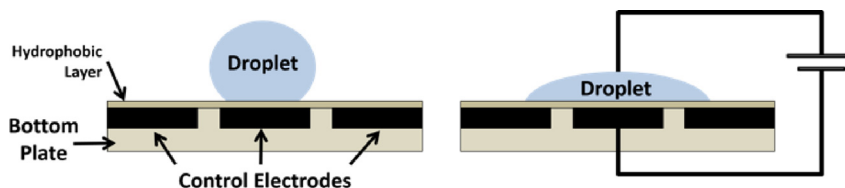

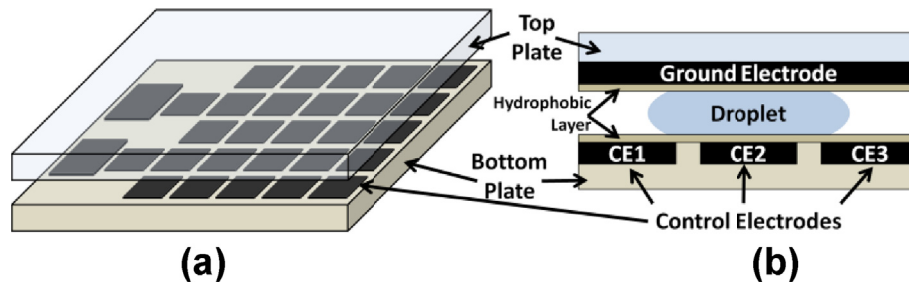**Fig. 1.** Illustration of the electrowetting effect.

Fig. 2. Depiction of a DMFB, including an optional top plate/ground electrode.
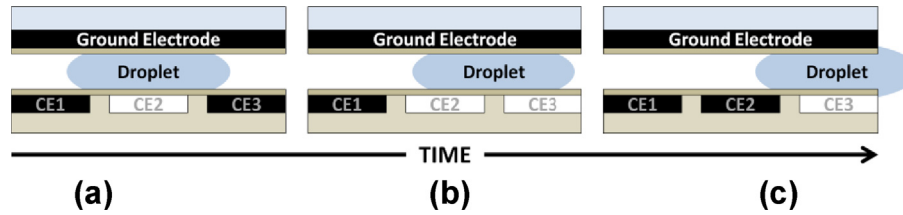

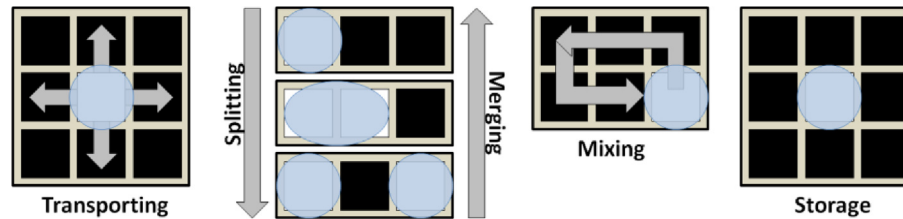**Fig. 3.** Depiction of a DMFB, including an optional top plate/ground electrode.

Fig. 4. A DMFB ISA contains five basic operations.
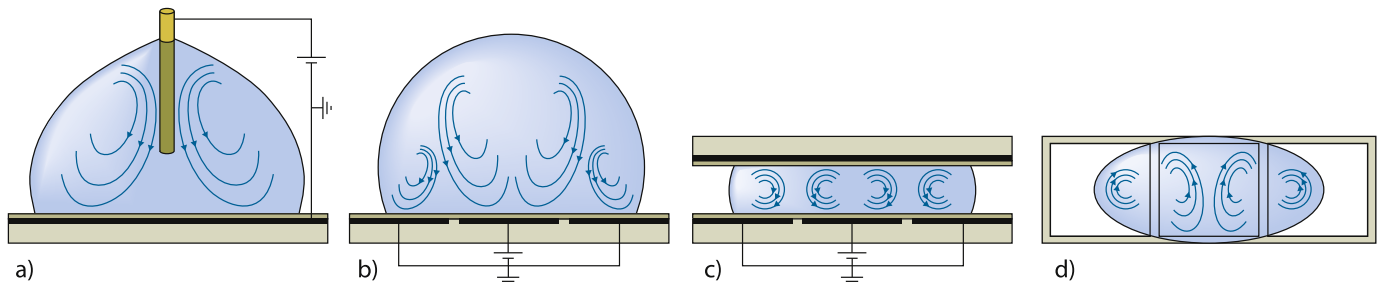

Fig. 5. Stationary mixing using a wire (a), three parallel electrodes with no top plate (b) and three parallel electrodes with a top-plate (c, d).[14, Fig. 3(i)–(iii)].

wires onto additional PCB layers; this impact can be tempered with algorithmic enhancements that synergistically optimize pin sharing with escape routing [37,38].

The vast majority of pin-sharing schemes that have been proposed previously produce application-specific designs [37–39]. One exception is called a Field-Programmable Pin-Constrained (FPPC) DMFB [36,40], which was general-purpose and could be fabricated with one or two PCB layers depending on the PCB technology parameters and the amount of flexibility build into the droplet transport busses. Due to these favorable properties we introduce a Stationary Mixing (SM-) FPPC DMFB and evaluate its cost and performance.

Fig. 6 depicts two variants of the SM-FPPC DMFB. These designs each contain four work modules that perform (stationary) mixing, splitting, merging, and storage. Three busses (two horizontal, one vertical) transport droplets between the work modules and between work modules and I/O reservoirs on the perimeter of the chip.

The "Pin-optimized" SM-FPPC in Fig. 6(a) employs two three-phase

busses, each of which requires 3 electrodes. The advantage of this approach is that few control pins (9 in total) are required; the disadvantage is that it becomes difficult to simultaneously transport more than one droplet per bus in parallel. To improve routing performance, the "Route-optimized" SM-FPPC in Fig. 6(b) employs a direct addressing bus (32 pins in total) that can route multiple droplets in parallel.

Work module I/O, splitting, and merging operations are effectively the same as for the original FPPC DMFB designs [36,40]; similarly, external devices such as heaters or optical detectors can be placed on the device above or below work modules. We omit a detailed discussion of these issues for brevity. There are substantial differences for stationary mixing and storage operations, which are discussed in detail next.

Stationary Mixing: Referring back to Fig. 6, independently addressable Mixer-Store electrodes (light orange) perform stationary mixing in conjunction with shared-pin Mixing electrodes (light blue). Fig. 7 depicts independent stationary mixing operations performed in conjunction with droplet storage, which is discussed next. Mixer-Store
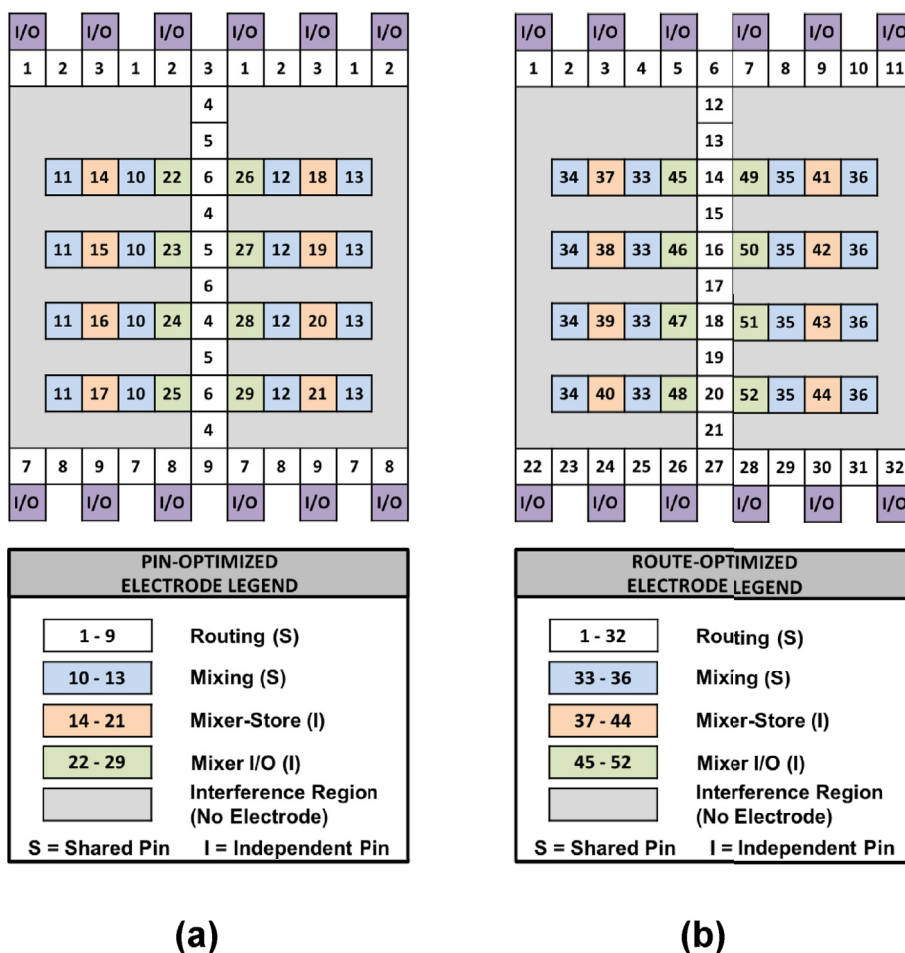
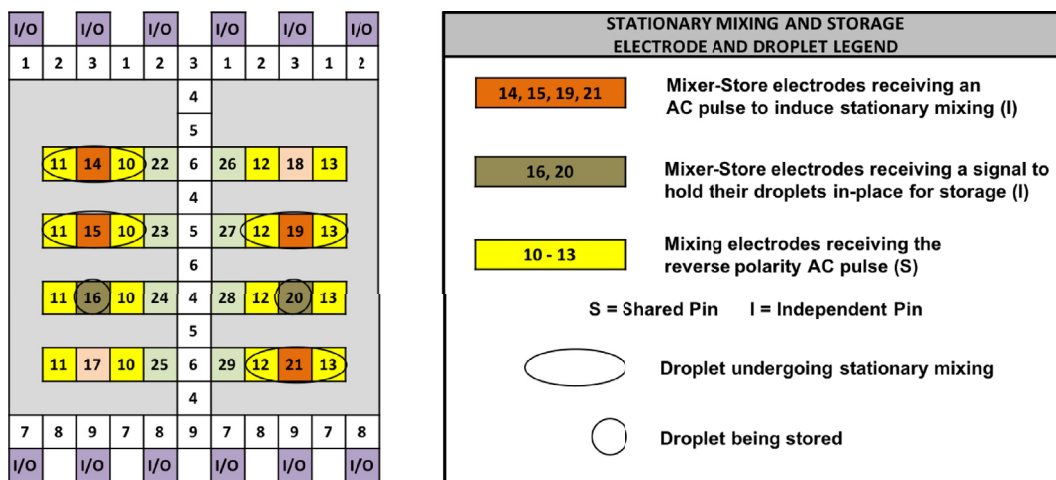**Fig. 6.** Pin-optimized (a) and Route-optimized (b) SM-FPPC DMFBs.

Fig. 7. An SM-FPPC performing four stationary mix operations concurrently with two droplet storage operations.

electrodes (**pins 14, 15, 19, and 20**; dark orange) receive AC voltage pulses with identical polarities, provided by an external power supply. All Mixing electrodes (**pins 11–13**, yellow) are driven to ground, but are connected to the Mixer-Store electrodes by capacitors underneath the chip, as shown in Fig. 5(b) and (c). This permits pin sharing among Mixing electrodes while ensuring that all independently addressable Mixer-Store electrodes being actively pulsed can induce stationary mixing.

Storage: As shown in Fig. 7, stationary mixing and storage can be performed concurrently by independently addressing Mixer-Store electrodes as appropriate. The Mixer-Store electrodes that perform storage (**pins 16 and 20**, brown) hold droplets in-place using standard AC voltages that typically perform basic DMFB operations [6,41]. Current ongoing stationary mixing operations minimally perturb the stored droplets, which are centered atop their respective Mixer-Store electrodes; stationary mixing, in contrast, spreads the droplet being mixed across

three consecutive electrodes, as shown in Fig. 5(c) and (d) and repeated in Fig. 7.

The last architectural issue to address is the number of PCB layers required to realize the SM-FPPC DMFB. Fig. 8 shows a manually-designed escape routing solution. Fig. 8(a) shows a design with eight work modules (four per side), while Fig. 8(b) extends the design to sixteen work modules (eight per side). The basic escape routing pattern for each group of four work modules (excluding the top and bottom horizontal busses) is repeatable, which indicates that the pin-optimized SM-FPPC DMFB can grow arbitrarily long in the vertical direction without additional PCB layers.

Fig. 9 shows a two-layer manually-designed escape routing solution for the route-optimized SM-FPPC DMFB. The first layer, in Fig. 9(a), routes control signals to the work modules, while the second layer, in Fig. 9(b), routes control signals to the transport busses. Both patterns are repeatable, thus the route-optimized SM-FPPC DMFB can grow arbitrarily long in the vertical direction without additional PCB layers.

5. SM-FPPC compiler

Compilation targeting a DMFB is a three-step process comprising scheduling, placement, and routing [42], as shown in Fig. 10.

Scheduling determines the times at which each operation starts and finishes [43–47].

Placement determines an on-chip location for each scheduled operation [48–51].

Routing determines the paths droplets take as they are routed between scheduled and placed operations [52–59]. The router may also introduce wash droplets to prevent cross-contamination [60–62].

The original FPPC DMFB employed two distinct work module types: Mixing modules (which only perform mixing) and Split-Storage-Detect (SSD) modules which perform all other operations. The scheduler is aware of the number of modules of each type, as well as the set of available I/O reservoirs, and is thus resource constrained. The placer binds scheduled operations to capable work modules and appropriate I/O reservoirs for the given fluid. The router is highly restricted in terms of

path planning, as it can only route droplets using the three transport busses, and can only transport one droplet at a time on each bus when targeting the pin-optimized FPPC DMFB, and can introduce wash droplets when needed. Details are summarized in Ref. [36].

In contrast, the SM-FPPC DMFB contains a uniform work module that can perform all operations; the only feature that may distinguish work modules from one another is whether or not a module contains an external device, such as a heater or detector. It is straightforward to modify the scheduler and placer to account for this; details are omitted for brevity. The router, in contrast, is not concerned with the issue of module types: all that the router needs to know is the source and destination of each droplet to be routed, the location of I/O ports on the perimeter of the chip, and whether or not washing is required to eliminate cross-contamination.

5.1. Droplet routing: overview

Scheduling and placement are computed under the assumption that droplet routing is instantaneous. The router inserts a droplet transport operation each time a new scheduled operation begins or ends; all ongoing operations that have been scheduled are paused during routing [52]. Thus, total assay execution time comprises an interleaved sequence of scheduled operational phases (SO_i) and droplet routing phases (DR_i), as shown in Fig. 11. Although there has been at least one attempt to relax this constraint in recent years [63], this interleaved model remains prevalent; we attempt to optimize the model in the following subsections.

5.2. Concurrent droplet routing with three-phase busses

This section addresses the capabilities and limitations of the three-phase busses in the pin-optimized (SM-)FPPC DMFB. Specifically, the three-phase busses inhibit concurrent routing of droplets in opposite directions. As shown in Fig. 12(a), it is not possible to concurrently route two droplets in opposite directions on the three-phase bus. **Droplet #1**, which is routed downward, requires an activation sequence **4 5 6** …, while **Droplet #2** which is routed upward requires an activation

(a)   (b)
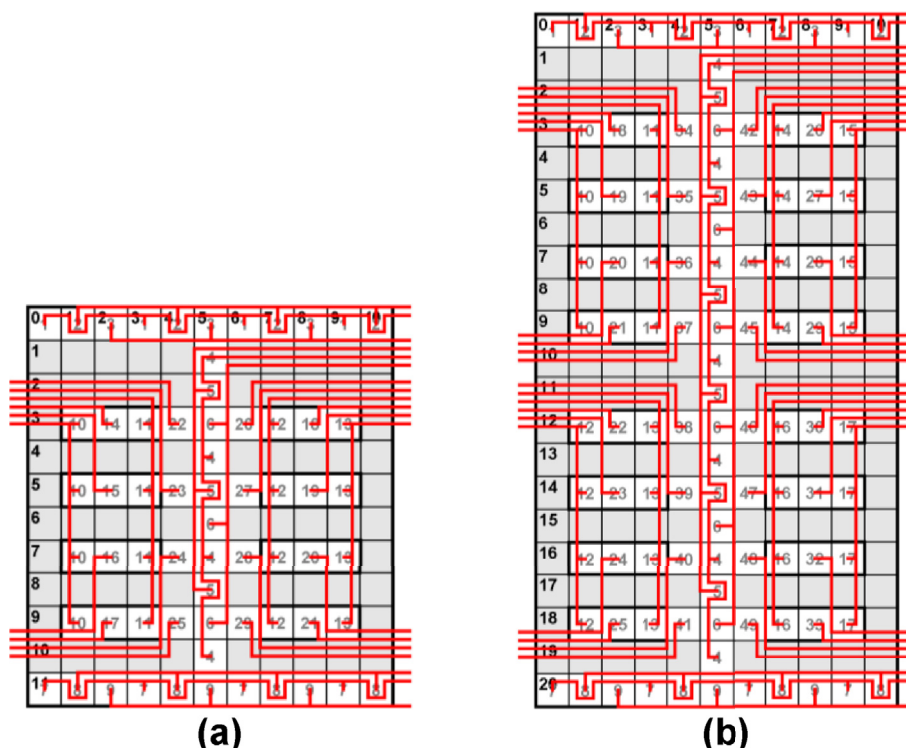
Fig. 8. Single-PCB layer escape routes for the pin-optimized SM-FPPC DMFB.
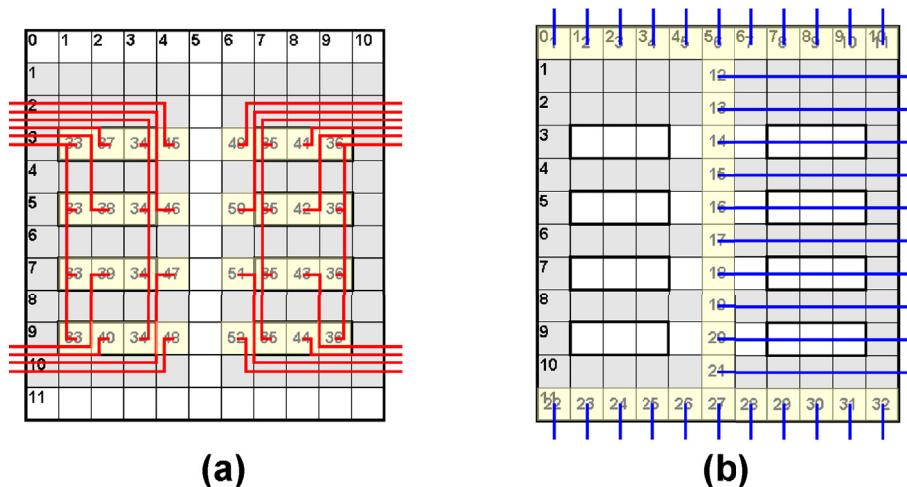
Fig. 9. Two-PCB layer escape routes for the route-optimized SM-FPPC DMFB.

Fig. 10. The three main stages of a DMFB compiler.

Fig. 11. A fully compiled bioassay is a sequence of interleaved operational phases (which are scheduled and placed) and droplet routing phases.

Fig. 12. Concurrent droplet routing in opposite directions is not possible using a three-phase bus (a) but becomes possible with a direct-addressing bus (b).

sequence **6 4 5** …, which are incompatible; in Fig. 12(b), both droplets can be routed concurrently using the route-optimized (SM-)FPPC DMFB, because all electrodes in the transport busses are addressed independently, which comes at a higher over all cost.

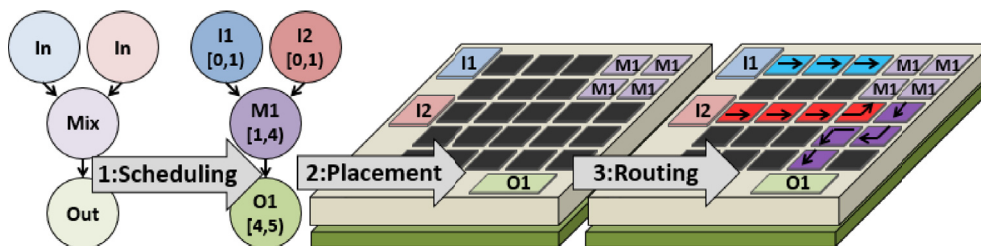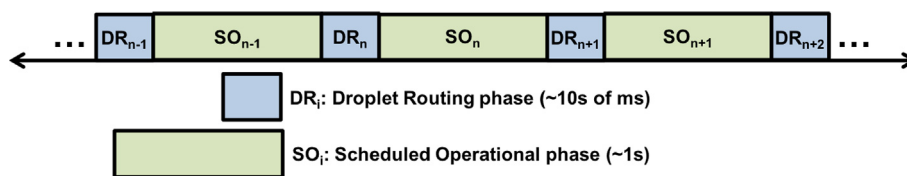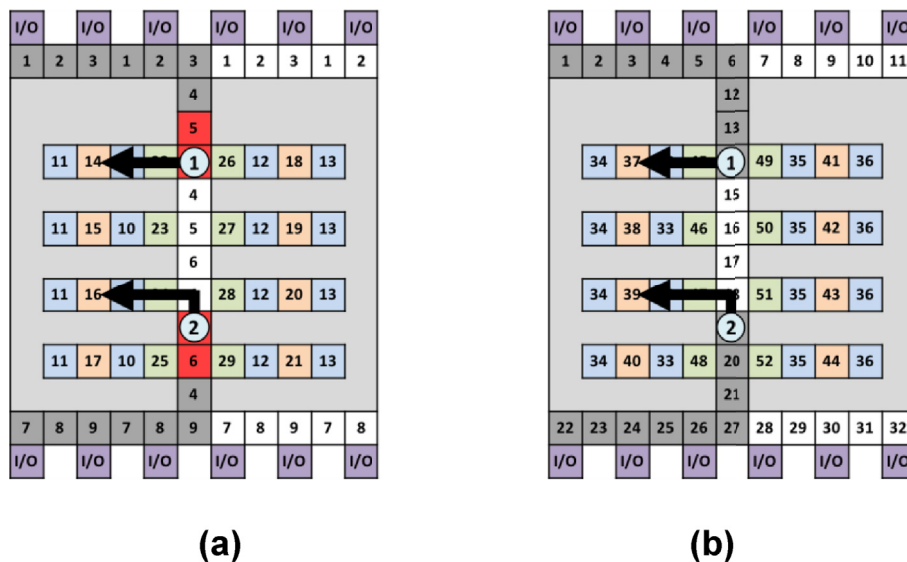In some cases, it may be possible to route droplets concurrently in the same direction on a three-phase bus, as shown in Fig. 13(a). In this case, both droplet routes share a common electrode activation subsequence, … **4 5 6** …, on the central three-phase bus. This is a very specific corner case that does not occur frequently in practice. A more common situation, as illustrated in Fig. 13(b), occurs when the work modules of two droplets connect to the three-phase bus at electrodes controlled by different pins: **pin #6** must be activated to draw **Droplet #1** into the central bus, which creates an incompatibility with **Droplet #2**; likewise, **pin #4** must be activated to draw **Droplet #2** into the central bus, which creates an incompatible with **Droplet #1**.

The situation can be rectified as follows. In Fig. 14(a), **Droplet #1** is first drawn into the central bus by activating **pin #6**, and is then transported down by one position by deactivating **pin #6** and activating **pin #4**. At this point, it is possible to draw **Droplet #2** into the bus by activating **pin #28**, however, **pin #4** must remain activated to hold **Droplet #1** in-place, as shown in Fig. 14(b). As a result, **Droplet #2** will be stretched across two adjacent electrodes, as shown in Fig. 14(c); at this point, deactivating **pin #28** will completely draw **Droplet #2** into the central bus, as shown in Fig. 14(d).

The drawback of this approach is that **Droplet #1** needs to wait while **Droplet #2** is drawn into the central bus, and in many situations, it may be simpler and faster to deliver **Droplet #1** to its target work module prior to drawing **Droplet #2** into the central bus. To simplify subsequent discussion, further routing optimizations will be described in the context of the route-optimized (SM-)FPPC DMFB.

Figs. 13(a) and 14 depict situations that are not the common case. Opportunities to route droplets concurrently using the three-phase bus architecture do not occur often in practice; as a result, the route-optimized (SM-)FPPC DMFB offers much higher routing performance than its pin-optimized counterpart.

5.3. Overlapping droplet routing with scheduled operational phases

Fig. 11 showed that that traditional approach to DMFB compilation interleaved scheduled assay operational phases with droplet routing phases. Here, we identify a set of relatively simple and straightforward situations in which certain droplet routes can be performed concurrently with scheduled operations, without adversely affecting assay execution. This shortens the latency of droplet routing phases if the route that has been chosen for reallocation lies on the critical path. We illustrate these opportunities using three examples.

Example 1: Input Droplet Optimization (Free Target Module). Fig. 15(a)–(c) shows two consecutive scheduled operational phases (SO_{n-1} and SO_n) of a bioassay with one interleaved droplet routing phase (DR_n). During SO_{n-1}, **Droplets #1** and **#2** are scheduled on their respective work modules; during DR_n, **Droplet #3** is routed from an input reservoir to a new work module; and during SO_n, **Droplets #1** and **#2** continue their scheduled operations, while **Droplet #3** begins its operation.

Fig. 15(d)–(f) illustrates the optimized outcome, which includes washing **Droplet #3**'s route is performed during SO_{n-1}, concurrently with the scheduled operations that process **Droplets #1** and **#2**; no droplets are routed during DR_n, dropping its latency to zero; and during SO_n, a wash droplet is routed to decontaminate Droplet #3's routing path, while all three droplets undergo scheduled operations. In this example, the time required to route Droplet #3 and the wash droplet are far less than the respective latencies of SO_{n-1} and SO_n; the general strategy is to route Droplet #3 toward the end of SO_{n-1} and the wash droplet toward the beginning of SO_n. This frees up time at the beginning of SO_{n-1} to perform any concurrent droplet routing/washing arising from DR_{n-1} (not shown), and time at the end of SO_{n+1} to perform any concurrent droplet routing arising from DR_{n+1} (also not shown).

Example 2: Input Droplet Optimization (Occupied Target Module). Fig. 16(a)–(c) shows an example similar in principle to Fig. 15(a)–(c), but with one subtle change: **Droplet #3**'s target module is presently occupied by **Droplet #2**, which necessitates routing **Droplet #2** out of the way before **Droplet #3** can be routed.

Fig. 16(d)–(f) illustrates the opportunities for concurrent droplet routing. During SO_{n-1}, **Droplet #3** is routed to a free work module nearby its target, and **Droplet #3**'s routing path is washed. This shortens the routing path from **Droplet #3** during DR_n, while ensuring that **Droplet #2** has a decontamination-free path from its source to target. **Droplets #2** and **#3** are then routed during DR_n, whose latency is reduced by **Droplet #3**'s shorter routing path. Washing **Droplet #3**'s routing path is deferred until SO_n.

Example 3: Deferred wash droplet routing. Fig. 17(a)–(c) shows an
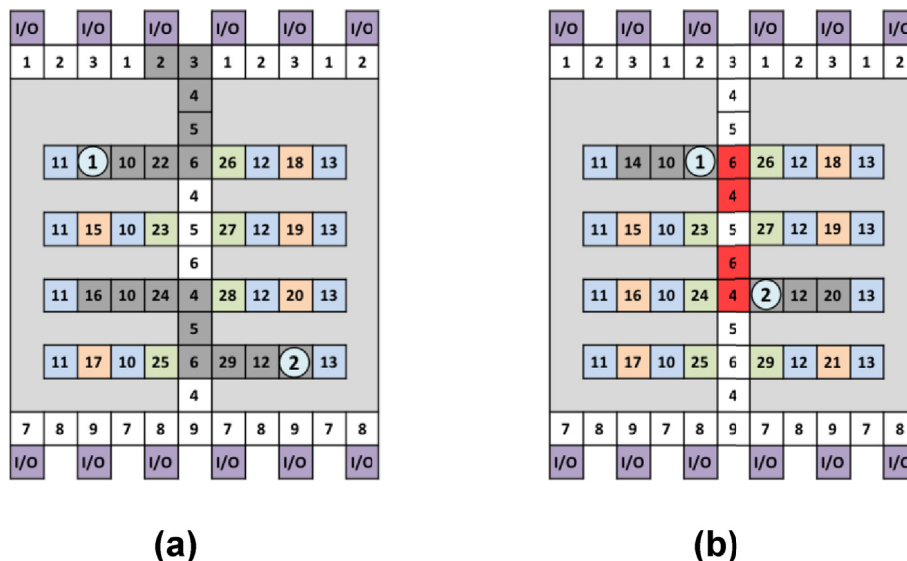

(a)　　　　　　　　　　　　　　　　　　　**(b)**

Fig. 13. In the route-optimized (SM-)FPPC DMFB, two droplets can route in the same direction on a three-phase bus if they share a common activation sequence (a). Concurrent routing is not possible if the central bus electrodes adjacent to the respective source work modules are driven by different pins (b).
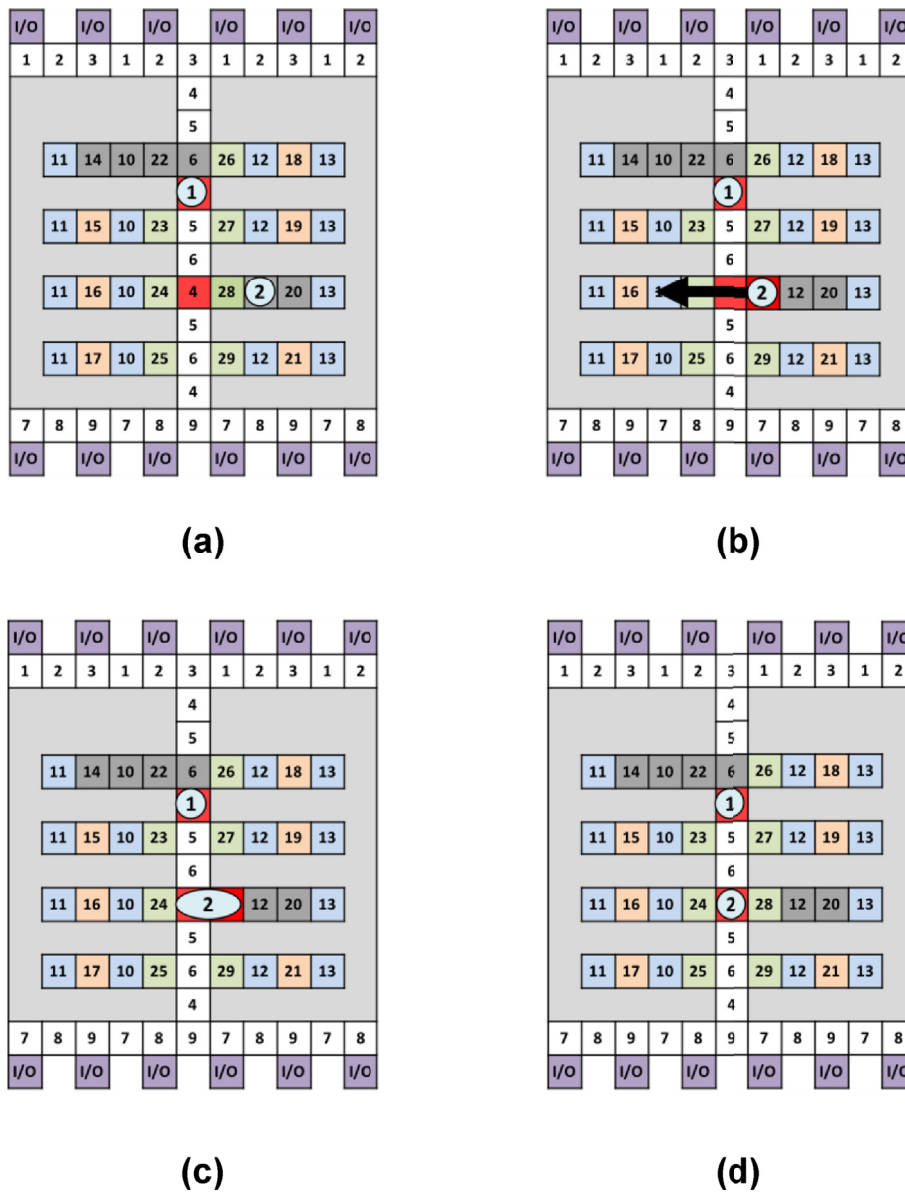
(a)

(b)

(c)

(d)

Fig. 14. I/O procedure to enable concurrent droplet routing in the same direction using a three-phase transport bus.

example that starts with three droplets undergoing scheduled operations during SO_{n-1}. **Droplet #2** is routed to a new work module during DR_n. **Droplets #1** and **#3** continue their operations and **Droplet #2** starts a new operation during SO_n. In Fig. 17(d)–(f), **Droplet #2**'s route must still be performed during DR_n, but the corresponding washing step can be deferred until SO_n, thereby reducing the overall latency of DR_n.

Example 4 Droplet Output Optimization. Fig. 18(a)–(c) shows an example that starts with three droplets undergoing scheduled operations during SO_{n-1}. **Droplet #2** is routed to an output reservoir during DR_n, and **Droplets #1** and **#3** continue their operations during SO_n. In Fig. 18(d)–(f), **Droplet #3**'s route, and its wash droplet route, are deferred to SO_n, which eliminates the need to route any droplets during DR_n.

Although the four examples shown in Figs. 15–18 are special cases, they elucidate a more general strategy for overlapping droplet routing with scheduled assay operations. This strategy can easily generalize to multiple droplets, although a detailed discussion of precisely how to do so is omitted for brevity. As in the discussion of the three examples, DR_n refers to the current droplet routing phase, while SO_{n-1} and SO_n refer to

the scheduled operational phases immediately before and after DR_n.

- A droplet can be routed concurrently with scheduled operations in SO_{n-1} if it is ready (i.e., it does not need to wait for an operation scheduled during SO_{n-1}) and a suitable unoccupied and uncontaminated target location can be identified.
- A droplet can be routed concurrently with scheduled operations in SO_n if it is not scheduled to perform an operation during SO_n and a suitable unoccupied and uncontaminated target location can be identified.

Wash droplet routing can easily be integrated into this strategy:

- If a droplet is routed concurrently with scheduled operations in SO_{n-1}, then its path should be washed during SO_{n-1} as well.
- If a droplet is routed during DR_n, and no subsequent droplets are routed along its path, then its path can be washed concurrently with scheduled operations in SO_n.
- If a droplet is routed concurrently with scheduled operations in SO_n, then its path can be washed during SO_n as well.
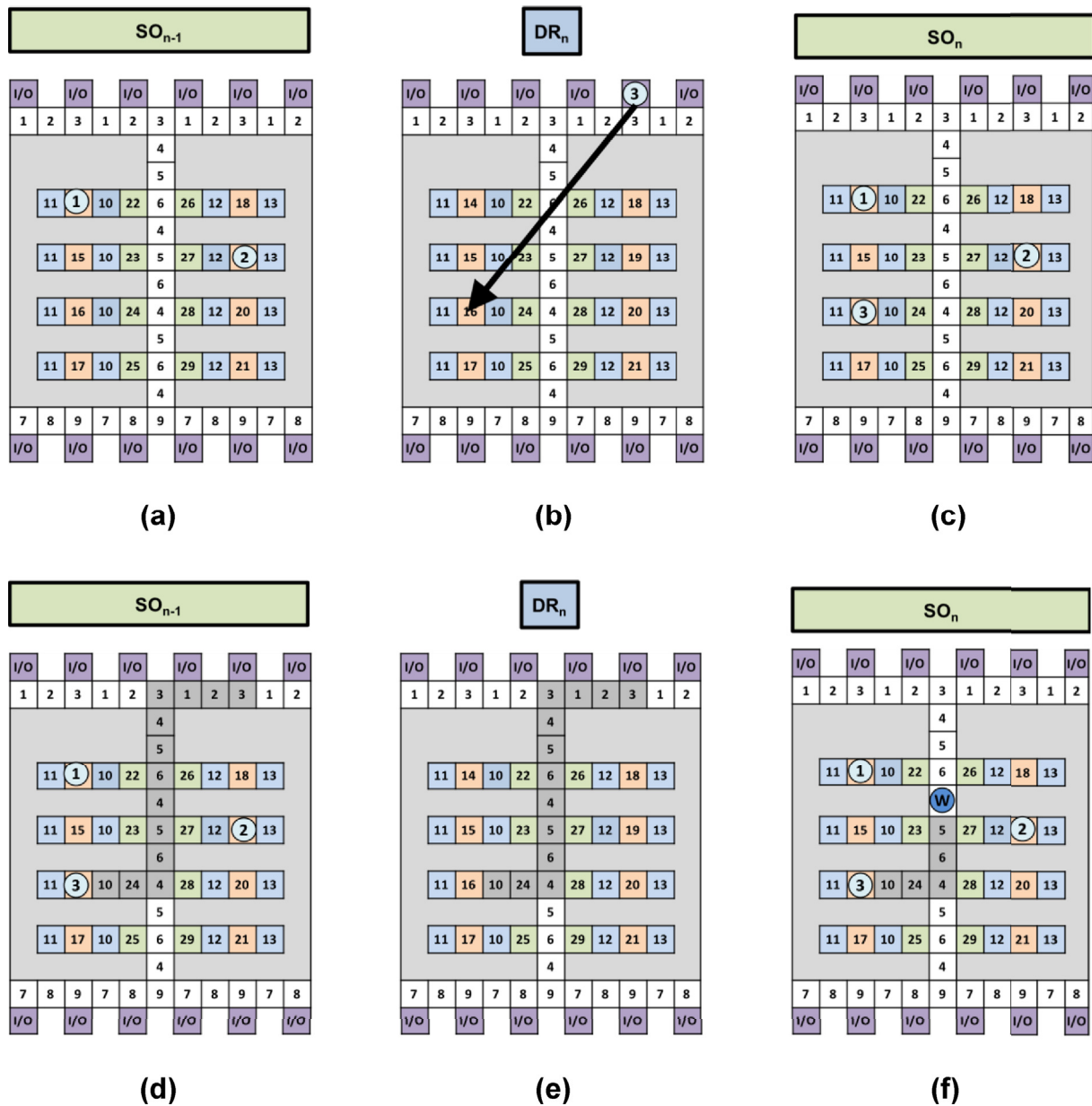
Fig. 15. Droplet routing interleaved with scheduled operational phases (a)–(c); droplet routing overlapping scheduled operational phases (d)–(f).

The key algorithmic challenge is to select the optimal suitable unoccupied and uncontaminated target location for each droplet. In the case of the (SM-)FPPC DMFB, the optimal location would be the unoccupied work module closest to the target, with ties broken arbitrarily. The problem becomes harder when extended to handle multiple droplets with multiple targets, or to generalize it to direct addressing DMFBs in which reconfigurable operations can be placed at any location on-chip.

6. Simulation results

We compare the proposed SM-FPPC DMFB to several previously technologies and architectures: (1) Direct Addressing (DA); (2) the pin-optimized FPPC featuring 1 and 3 vertical busses (FPPC-P1, FPPC-P3); and (3) the route-optimized FPPC featuring 1 and 3 vertical busses (FPPC-R1, FPPC-R3).

Table 1 summarizes the architectural differences between the chosen targets. DA uses a large 15×19 array, which integrates eight optical detectors. The compiler is optimized for speed, rather than performance, and uses a virtual topology, comprising an array of 4×3 work modules,

which simplifies both placement and routing [64]; these algorithms are similar in principle to those used by the compiler that targeted the FPPC in prior work [36] and the SM-FPPC here.

The FPPC-(P/R, 1/3) variants, which are smaller than DA in terms of area, integrate four modules for mixing, and six modules that perform storage, splitting, and detection [36,40]; the SM-FPPC includes a smaller uniform module type, due to stationary mixing, has the smallest area and integrates eight optical detectors in an 11×12 array.

6.1. PCB cost

Table 2 reports the number of control pins, number of shift registers, number of PCB layers, and width/height of a PCB generated for each DMFB architecture listed in Table 1; in addition, DA chips with varying dimensions are reported, along with the pin- and route-optimized SM-FPPCs, denoted SM-FPPC-(P/R). The requirements reported in Table 2 were computed as described previously by Grissom et al. [36].

Fig. 19 reports total cost estimates, which include the cost of the PCB added to the cost of the shift registers that are mounted on the PCB to
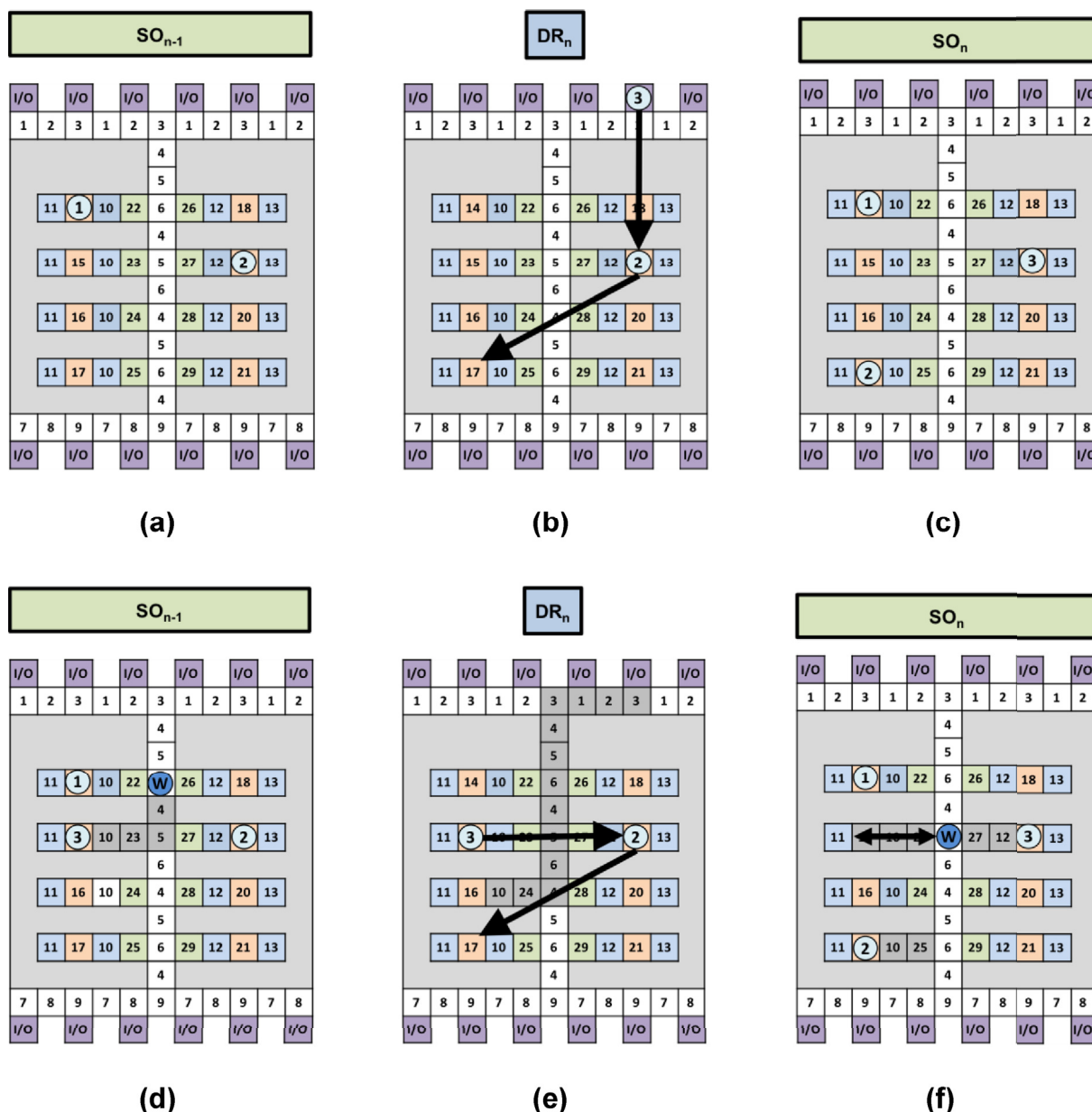
Fig. 16. Droplet routing interleaved with scheduled operational phases (a)–(c); droplet routing overlapping scheduled operational phases, yielding shorter droplet routes and concurrent washing (d)–(f).

deliver signals to the DMFB; PCB cost estimates were obtained using Advanced Circuits' instant online quote [65]. The SM-FPPC-P is the cheapest option, followed by FPPC-P1 and SM-FPPC-R. The two cheapest chips benefit from two factors: the usage of a single vertical routing bus (as opposed to three, in the case of FPPC-(P/R)3, and the choice pin-optimized (3-phase), rather than route-optimized (direct addressing) transport busses.

All three DA chips were considerably more expensive than any of the FPPC variants. Thus, the flexibility and reconfigurability inherent in DA architectures comes at a significant cost compared to the FPPC variants, all of which are programmable, but in a far more constrained way. The key cost benefit of the SM-FPPC variants is that stationary mixers require 3 electrodes, where the FPPC-(P/R)(1/3) variants employ larger 4×2 mixers. These costs include PCBs and shift registers, and do not include the cost of additional equipment, as the SM-FPPC requires an external power supply to provide AC voltage. In practice, the PCB-mounted DMFBs are disposable, so the cost of the external power supply will be amortized over a large number of runs.

6.2. SM-FPPC performance

Fig. 20 reports the total bioassay execution times for eight benchmark assays that are widely used to evaluate the performance of DMFB compilers; the implementation was performed using the open source UCR Static Synthesis Simulator [42]. The comparison includes DA (15×19) and the pin-optimized FPPC-P1, FPPC-P3, and SM-FPPC-P DMFBs. All droplet transport operations were performed during distinct droplet routing phases. The simulator supports wash droplet routing for all (SM-) FPPC variants, but not DA; thus wash droplet routing is not performed in these experiments.

In all cases, SM-FPPC-P yielded the fastest overall execution times, which can be attributed primarily to the fact that stationary mixing operations take 1 s while transport-based mixing operations take 3 s; the FPPC-P(1/3) chips integrate fewer detectors than the In all but one case (InVitro-2), the SM-FPPC-P achieved shorter droplet router latencies than the FPPC-P(1/3) variants; however, for all benchmarks, DA yielded the fastest overall droplet routing times, which can be attributed to its
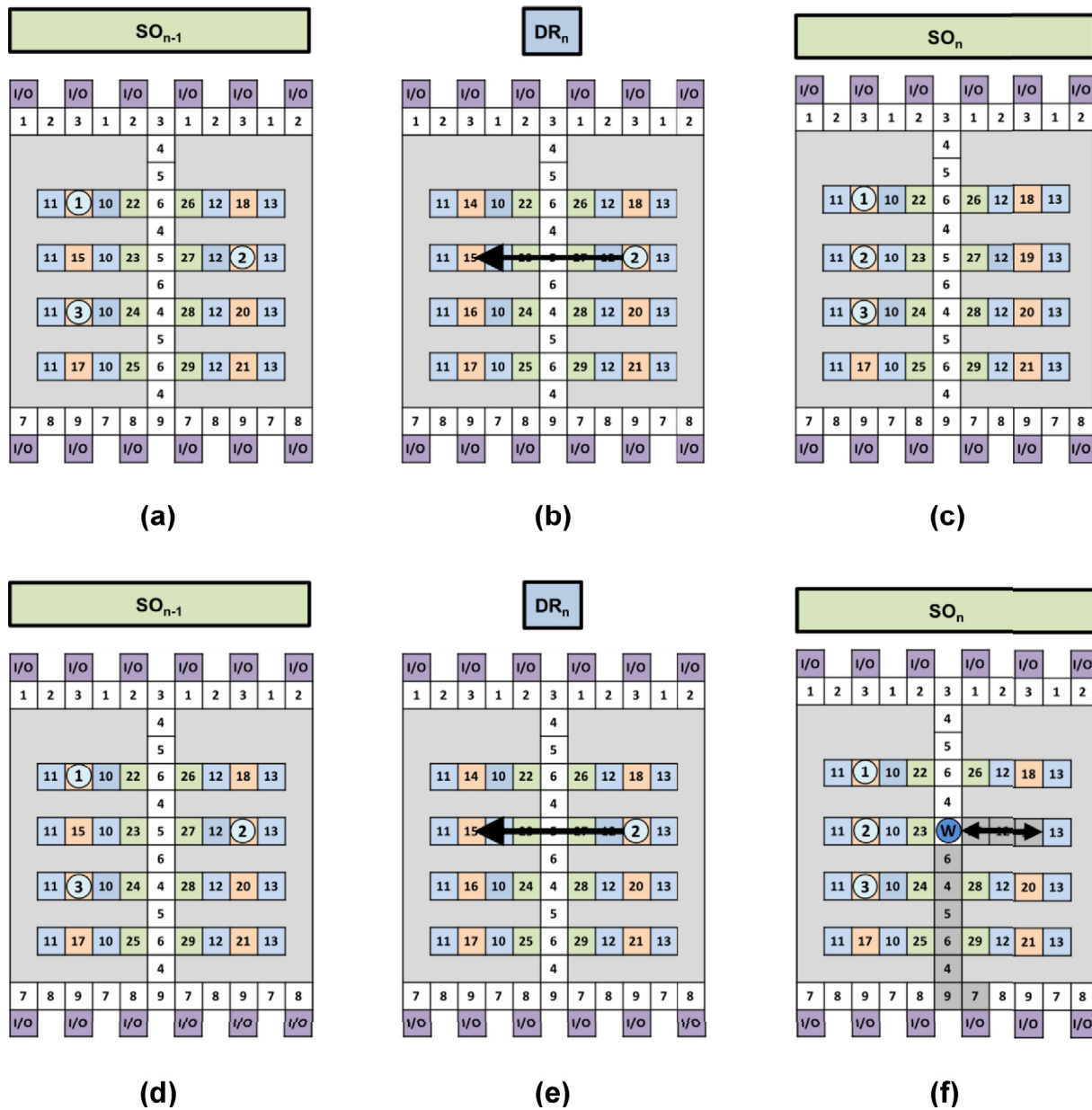
Fig. 17. Droplet routing interleaved with scheduled operational phases (a)–(c); droplet routing overlapping scheduled operational phases; the wash droplet route overlaps the scheduled operational phase after the droplet routing phase.

greater flexibility and reconfigurability, as droplets are not restricted to being routed on architecturally-defined 3-phase transport busses.

To summarize, these experiments have quantified the benefits of stationary mixing over rotation-based mixing in a low-cost PCB-mounted platform: on average, the SM-FPPC executes assays $1.50\times$ faster than DA and $1.39\times$ faster than both FPPC-P(1/3).

6.3. Performance impact of overlapping droplet routing with scheduled operational phases

Fig. 21 reports the performance impact of overlapping droplet routing with scheduled operational phases on bioassay execution time. These experiments were performed using the SM-FPPC-P DMFB with wash droplet routing enabled. The bars labeled "Traditional" refer to the baseline approach in which all droplet routes are performed during droplet routing phases; the bars labeled "Optimized" allow certain droplet routes to be performed concurrently with scheduled operational phases, as discussed in detail in Section 5.3. Droplet routing times have a

much greater impact on the reported bioassay execution times for the SM-FPPC-P in Fig. 21, compared to Fig. 20, where droplet routing was disabled.

On average, optimized routing sped up droplet routing times by $1.37\times$, and bioassay execution time by $1.08\times$. Although these speedups are admittedly quite modest, they require no hardware modifications at all, and thus incur no extra cost. Additionally, noting that the optimized droplet routing was evaluated for the SM-FPPC-P DMFB, similar trends were observed for the SM-FPPC-R and FPPC-(P/R)(1/3) DMFBs as well; details have been omitted for brevity.

7. Related work

The choice to employ stationary mixing does impose some technological constraints on the system which cannot and should not be ignored. Before discussing those details, it is important to recognize that DMFBs are inherently error prone and have relatively short lifetimes [66], and each PCB will be discarded after a single use. Thus, the cost of

Fig. 18. Droplet routing interleaved with scheduled operational phases (a)–(c); Droplet #2 can be routed concurrently with ongoing assay operations (d), eliminating the need to route it during the droplet routing phase (e); the routing path can be washed concurrently with the next scheduled operational phase (f).

Table 1
Architectural parameters for the DMFBs used in the reported experiments.

DA		FPPC-(P/R)1		FPPC-(P/R)3		SM-FPPC	
Dimensions	Detectors	Dimensions	Mixers/Detectors	Dimensions	Mixers/Detectors	Dimensions	Work Modules
15×19	8	10×16	4/6	12×15	4/6	10×10	8

the PCB is quite important as many will typically be used to carry out a scientific study; that said, the cost of the external operating equipment should not be ignored. This may change with the advent of inkjet-printed electronics as it may soon be possible to print the electrodes on paper [67–69], which may be affixed to a PCB-based control system [70]; in such a platform, the paper, but not the PCB, would be disposable.

Stationary mixing requires AC voltages, which has implications for both cost and performance. For example, the University of Toronto/Sci-Bot DropBot platform uses AC voltages, which necessitates an external power supply that is much larger than the actual DMFB platform [71].

DropBot fabricates electrodes by vapor-deposition on a chromium substrate, and employs a costly nanocoating step to ensure hydrophobicity. The cost of the entire platform is $500, although replacement DMFBs alone are likely to cost far less. In contrast, Gaudi Labs' OpenDrop platform uses DC current, is PCB-based, features a high-voltage switch, regulator, control circuit, and step-up voltage converter as PCB-mounted components, and uses thin film and oil for coating, all at a cost of $10 [6]. Adding stationary mixing capabilities to a platform like OpenDrop would significantly increase the cost of its operating equipment, even if the PCB-based part was disposable.

Table 2
PCB requirements for the DMFB architectures listed in Table 1.

DMFB Architecture	Pins	Shift Registers	PCB Layers	Width (in.)	Height (in.)
DA (15 × 19)	285	33	3	4.55	1.75
DA (15 × 15)	225	25	3	3.44	1.59
DA (10 × 10)	100	9	2	2.13	1.39
FPPC-R1	61	5	2	1.76	1.63
FPPC-P3	33	1	4	1.84	1.59
FPPC-R3	60	4	2	1.84	1.59
SM-FPPC-R	52	3	2	1.8	1.47
FPPC-P1	36	1	2	1.76	1.63
SM-FPPC-P	29	0	2	1.43	1.47

On the other hand, there are several purely technological arguments in favor of AC voltage actuation over DC [41]. The first is that threshold voltages required to actuate droplets are lower for AC, except when the actuation frequency is greater than ~150 Hz; moreover, the difference between AC and DC actuation voltages at higher frequencies was minimal. Additionally, applying a DC voltage induced hysteresis in the droplet, whereas no hysteresis was observed when using AC voltages. Although these arguments do not account for cost, they do speak directly to correctness and feasibility when evaluating DMFB technology for a new application domain.
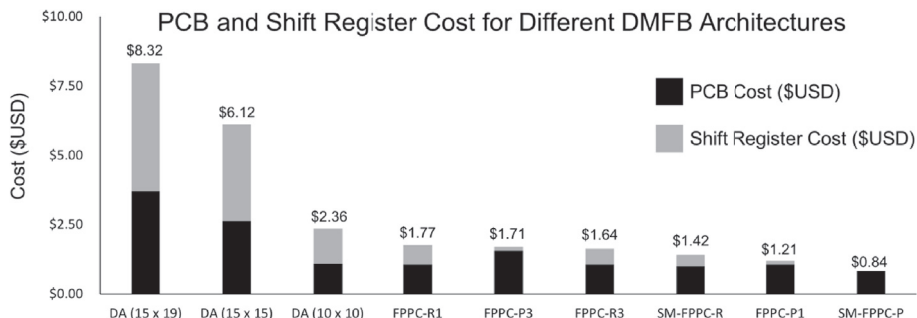

Fig. 19. Cost estimates for the PCBs (including shift registers) listed in Table 2.
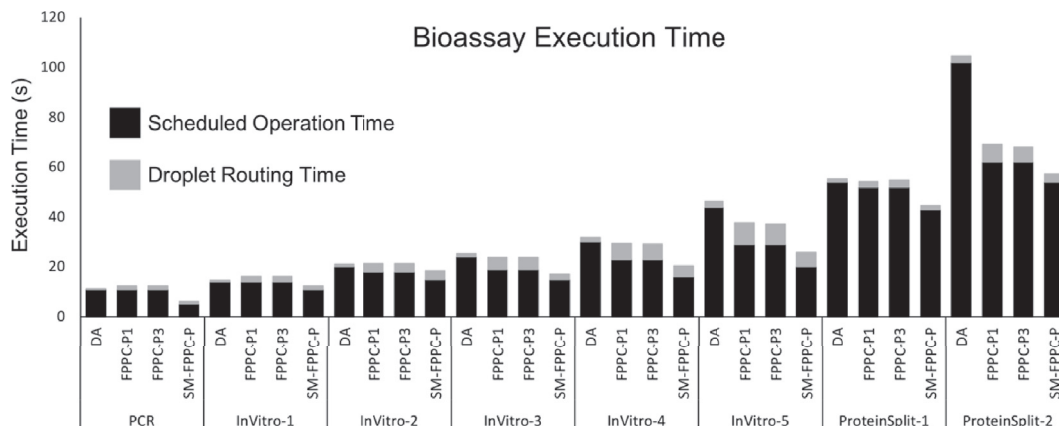

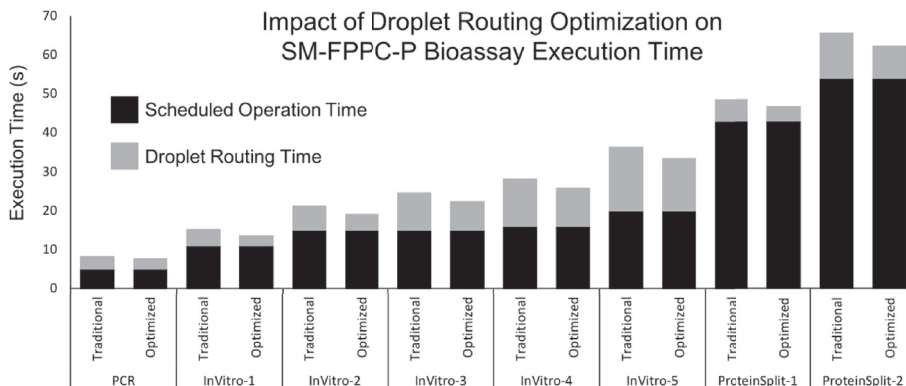Fig. 20. Bioassay execution time for eight benchmarks targeting four DMFBs.

Fig. 21. Impact of droplet routing optimization (overlapping some routes with scheduled operation phases) on droplet routing time and bioassay execution time for the SM-FPPC-1 DMFB with wash droplet routing enabled.

8. Conclusion

Previous work has shown that stationary mixing yields faster mixing times that rotation-based mixing and avoids the drawbacks associated with transporting droplets during mixing. This paper has described a pin assignment scheme to introduce stationary mixing in a low-cost general-purpose pin-constrained DMFB architecture, the SM-FPPC DMFB; the pin-optimized variant can be realized in a single PCB layer at a cost of $0.84 per chip, while the route-optimized variant, which requires more control pins, can be realized in two PCB layers at a cost of $1.42 per chip. This paper described the necessary steps that a compiler that targets the SM-FPPC DMFB must take, and introduced an optimization strategy for droplet routing and washing that allows concurrent execution of scheduled assay operations with droplet routing steps that satisfy specific constraints; this reduced bioassay execution time by $1.08\times$, on average, as a pure software enhancement that does not require any hardware modifications that could increase the cost of the device.

Acknowledgment

References

[1] Michael G. Pollack, Alexander D. Shenderov, Richard B. Fair, Electrowetting-based actuation of droplets for integrated microfluidics, Lab-on-a-Chip 2 (2) (2002) 96–101.

[2] Hyejin Moon, Sung Kwon Cho, Robin L. Garrell, Chang-Jin Kim, Low voltage electrowetting-on-dielectric, J. Appl. Phys. 92 (7) (2002) 4080–4087.

[3] Jian Gong, Chang-Jin Kim, Direct-referencing two-dimensional array digital microfluidics using multilayer printed circuit board, J. Microelectromech. Syst. 17 (2) (2008) 257–264 (2008).

[4] Joo Hyon Noh, Jiyong Noh, Eric Kreit, Jason Heikenfeld, Philip D. Rack, Toward active-matrix lab-on-a-chip: programmable electrofluidic control enabled by arrayed oxide thin film transistors, Lab-on-a-Chip 2 (2) (2012) 353–360.

[5] B. Hadwen, G.R. Broder, D. Morganti, A. Jacobs, C. Brown, J.R. Hector, Y. Kubota, H. Morgan, Programmable large area digital microfluidic array with integrated droplet sensing for bioassays, Lab-on-a-Chip 12 (18) (2012) 3305–3313 (2012).

[6] Mirela Alistar, Urs Gaudenz, OpenDrop: an integrated do-it-yourself platform for personal use of biochips, Bioengineering 4 (2) (2017) E45.

[7] Frieder Mugele, Jean-Christophe Baret, Electrowetting: from basics to applications, J. Phys. Condens. Matter 17 (28) (2005) R705.

[8] M.G. Pollack, P.Y. Paik, A.D. Shenderov, V.K. Pamula, F.S. Dietrich, R.B. Fair, Investigation of electrowetting-based microfluidics for real-time pcr applications, in: MicroTAS, 2013, pp. 619–622.

[9] Richard B. Fair, Andrey Khlystov, Tina D. Tailor, Vladislav Ivanov, Randall D. Evans, Vijay Srinivasan, Vamsee K. Pamula, Michael G. Pollack, Peter B. Griffin, Jack Zhou, Chemical and biological applications of digital-microfluidic devices, IEEE Des. Test Comput. 24 (1) (2007) 10–24.

[10] Sumit Kalsi, Martha Valiadi, Maria-Nefeli Tsaloglou, Lesley Parry-Jones, Adrian Jacobs, Rob Watson, Carrie Turner, Robert Amos, Ben Hadwen, Jonathan Buse, Chris Brown, Mark Sutton, Hywel Morgan, Rapid and sensitive detection of antibiotic resistance on a programmable digital microfluidic platform, Lab-on-a-Chip 15 (2015) 3065–3075.

[11] Mohamed Ibrahim, Craig Boswell, Krishnendu Chakrabarty, Kristin Scott, Miroslav Pajic, A real-time digital-microfluidic platform for epigenetics, in: CASES, 2016, pp. 10:1–10:10.

[12] J. Moore, M. Nemat-Gorgani, A.C. Madison, M.A. Sandahl, S. Punnamaraju, A.E. Eckhardt, M.G. Pollack, F. Vigneault, G.M. Church, R.B. Fair, M.A. Horowitz, P.B. Griffin, Automated electrotransformation of escherichia coli on a digital microfluidic platform using bioactivated magnetic beads, Biomicrofluidics 11 (1) (2017), 014110.

[13] Mohammad Paknahad, Ali Ahmadi, Jacques Rousseau, Hojatollah Rezaei Nejad, Mina Hoorfar, On-chip electronic nose for wine tasting: a digital microfluidic approach, IEEE Sensor. J. 17 (14) (2017) 4322–4329.

[14] Ehsan Samiei, Maria Diaz de Leon Derby, Andre Van den Berg, Mina Hoorfar, An electrohydrodynamic technique for rapid mixing in stationary droplets on digital microfluidic platforms, Lab-on-a-Chip 17 (2) (2017) 227–234.

[15] Phil Paik, Vamsee K. Pamula, Richard B. Fair, Rapid droplet mixers for digital microfluidic systems, Lab-on-a-Chip 3 (4) (2003) 253–259.

[16] Jie Ding, Krishnendu Chakrabarty, Richard B. Fair, Scheduling of microfluidic operations for reconfigurable two-dimensional electrowetting arrays, IEEE Trans. CAD Integr. Circuits Syst. 20 (12) (2001) 1463–1468.

[17] H. Ren, R.B. Fair, M.G. Pollack, Automated on-chip droplet dispensing with volume control by electrowetting actuation and capacitance metering, Sensor. Actuator. B Chem. 98 (2–3) (2004) 319–327.

[18] Vijay Srinivasan, Vamsee K. Pamula, Richard B. Fair, Droplet-based microfluidic lab-on-a-chip for glucose detection, Anal. Chim. Acta 507 (1) (2004) 145–150.

[19] Jian Gong, Chang-Jin Kim, All-electronic droplet generation on-chip with real-time feedback control for EWOD digital microfluidics, Lab-on-a-Chip (6) (2008) 898–906.

[20] Steve C.C. Shih, Ryan Fobel, Paresh Kumar, Aaron R. Wheeler, A feedback control system for high-fidelity digital microfluidics, Lab-on-a-Chip 11 (3) (2011) 535–540.

[21] Saman Sadeghi, Huijiang Ding, Gaurav J. Shah, Supin Chen, Pei Yuin Keng, Chang-Jin Kim, R.Michael van Dam, On chip droplet characterization: a practical, high-sensitivity measurement of droplet impedance in digital microfluidics, Anal. Chem. 84 (4) (2012) 1915–1923.

[22] Michael J. Schertzer, Ridha Ben Mrad, Pierre E. Sullivan, Automated detection of particle concentration and chemical reactions in EWOD devices, Sensor. Actuator. B Chem. 164 (1) (2012) 1–6.

[23] Miguel Angel Murran, Homayoun Najjaran, Capacitance-based droplet position estimator for digital microfluidic devices, Lab-on-a-Chip 12 (11) (2012) 2053–2059.

[24] Lin Luan, Matthew W. Royal, Randall Evans, Richard B. Fair, Nan M. Jokerst, Chip scale optical microresonator sensors integrated with embedded thin film photodetectors on electrowetting digital microfluidics platforms, IEEE Sensor. J. 12 (6) (2012) 1794–1800 (2012).

[25] Thomas Lederer, Stefan Clara, Bernhard Jakoby, Wolfgang Hilber, Integration of impedance spectroscopy sensors in a digital microfluidic platform, Microsyst. Technol. 18 (7–8) (2012) 1163–1180.

[26] Biddut Bhattacharjee, Homayoun Najjaran, Droplet sensing by measuring the capacitance between coplanar electrodes in a digital microfluidic system, Lab-on-a-Chip 12 (21) (2012) 4416–4423.

[27] Jie Gao, Xianming Liu, Tianlan Chen, Pui-In Mak, Yuguang Du, Mang-I. Vai, Bingcheng Lin, Rui P. Martins, An intelligent digital microfluidic system with fuzzy-enhanced feedback for multi-droplet manipulation, Lab-on-a-Chip 13 (3) (2013) 443–451.

[28] Steve C.C. Shih, Irena Barbulovic-Nad, Xuning Yang, Ryan Fobel, Aaron R. Wheeler, Digital microfluidics with impedance sensing for integrated cell culture and analysis, Biosens. Bioelectron. 42 (2013) 314–320.

[29] Matthew W. Royal, Nan M. Jokerst, Richard B. Fair, Droplet-based sensing: optical microresonator sensors embedded in digital electrowetting microfluidics systems, IEEE Sensor. J. 13 (12) (2013) 4733–4742.

[30] Yiyan Li, Hongzhong Li, R.Jacob Baker, Volume and concentration identification by using an electrowetting on dielectric device, in: DCAS, 2014, pp. 1–4.

[31] Yiyan Li, Hongzhong Li, R.Jacob Baker, A low-cost and high-resolution droplet position detector for an intelligent electrowetting on dielectric device, J. Lab. Autom. 20 (6) (2015) 663–669.

[32] Ehsan Samiei, Hojatollah Rezaei Nejad, Mina Hoorfar, Effect of electrode geometry on droplet splitting in digital microfluidic platforms, in: ASME ICNMM, 2014.

[33] Tao Xu, Krishnendu Chakrabarty, Integrated droplet routing and defect tolerance in the synthesis of digital microfluidic biochips, JETC 4 (3) (2008) 11:1–11:24.

[34] Tao Xu, Krishnendu Chakrabarty, Fei Su, Defect-aware high-level synthesis and module placement for microfluidic biochips, IEEE Trans. Biomed. Circuits Syst. 2 (1) (2008) 50–62.

[35] Elena Maftei, Paul Pop, Jan Madsen, Tabu search-based synthesis of dynamically reconfigurable digital microfluidic biochips, in: CASES, 2009, pp. 195–204.

[36] Daniel T. Grissom, Jeffrey McDaniel, Philip Brisk, A low-cost field-programmable pin-constrained digital microfluidic biochip, IEEE Trans. CAD Integr. Circuits Syst. 33 (11) (2014) 1657–1670.

[37] Jeffrey McDaniel, Zachary Zimmerman, Daniel T. Grissom, Philip Brisk, PCB escape routing and layer minimization for digital microfluidic biochips, IEEE Trans. CAD Integr. Circuits Syst. 36 (1) (2017) 69–82.

[38] Yang Zhao, Tao Xu, Krishnendu Chakrabarty, Broadcast electrode-addressing and scheduling methods for pin-constrained digital microfluidic biochips, IEEE Trans. CAD Integr. Circuits Syst. 30 (7) (2011) 986–999.

[39] Shih-Ying Sean Liu, Chung-Hung Chang, Hung-Ming Chen, Tsung-Yi Ho, ACER: an agglomerative clustering based electrode addressing and routing algorithm for pin-constrained EWOD chips, IEEE Trans. CAD Integr. Circuits Syst. 33 (9) (2014) 1316–1327.

[40] Daniel T. Grissom, Philip Brisk, A field-programmable pin-constrained digital microfluidic biochip, in: DAC, 2013, pp. 46:1–46:9.

[41] Isaac Nagiel, AC Electrowetting Actuation of Droplets on a Digital Microfluidic Platform, Duke University, 2007.

[42] Daniel T. Grissom, Christopher Curtis, Skyler Windh, Calvin Phung, Navin Kumar, Zachary Zimmerman, Kenneth O'Neal, Jeffrey McDaniel, Nick Liao, Philip Brisk, An open-source compiler and PCB synthesis tool for digital microfluidic biochips, Integration 51 (2015) 169–193.

[43] Andrew J. Ricketts, Kevin M. Irick, Narayanan Vijaykrishnan, Mary Jane Irwin, Priority scheduling in digital microfluidics-based biochips, in: DATE, 2006, pp. 329–334.

[44] Fei Su, Krishnendu Chakrabarty, High-level synthesis of digital microfluidic biochips, JETC 3 (4) (2008) 1:1–1:32.

[45] Chia-Hung Liu, Kuang-Cheng Liu, Juinn-Dar Huang, Latency-optimization synthesis with module selection for digital microfluidic biochips, in: SoCC, 2013, pp. 159–164.

[46] Abhimanyu Yadav, Trung Anh Dinh, Daiki Kitagawa, Shigeru Yamashita, ILP-based synthesis for sample preparation applications on digital microfluidic biocihps, VLSI Des. (2016) 355–360.

[47] Kenneth O'Neal, Daniel Grissom, Philip Brisk, Resource-constrained scheduling for digital microfluidic biochips, ACM JETC 14 (1) (2018) article #7.

[48] Fei Su, Krishnendu Chakrabarty, Module placement for fault-tolerant microfluidics-based biochips, ACM Trans. Des. Autom. Electron. Syst. 11 (3) (2006) 682–710.

[49] Ping-Hung Yuh, Chia-Lin Yang, Yao-Wen Chang, Placement of defect-tolerant digital microfluidic biochips using the T-tree formulation, JETC 3 (3) (2007) 13.
[50] Chen Liao, Shiyan Hu, Multiscale variation-aware techniques for high-performance digital microfluidic lab-on-a-chip component placement, IEEE Trans. NanoBioscience 10 (1) (2011) 51–58.
[51] Ying-Han Chen, Chung-Lun Hsu, Li-Chen Tsai, Tsung-Wei Huang, Tsung-Yi Ho, A reliability-oriented placement algorithm for reconfigurable digital microfluidic biochips using 3-D deferred decision making technique, IEEE Trans. CAD Integr. Circuits Syst. 32 (8) (2014) 1151–1162.
[52] Fei Su, William L. Hwang, Krishnendu Chakrabarty, Droplet routing in the synthesis of digital microfluidic biochips, in: DATE, 2006, pp. 323–328.
[53] Karl-Friedrich Böhringer, Modeling and controlling parallel tasks in droplet-based microfluidic systems, IEEE Trans. CAD Integr. Circuits Syst. 25 (2) (2006) 334–344.
[54] Eric J. Griffith, Srinivas Akella, Mark K. Goldberg, Performance characterization of a reconfigurable planar-array digital microfluidic system, IEEE Trans. CAD Integr. Circuits Syst. 25 (2) (2006) 345–357.
[55] Minsik Cho, David Z. Pan, A high-performance droplet routing algorithm for digital microfluidic biochips, IEEE Trans. CAD Integr. Circuits Syst. 27 (10) (2008) 1714–1724.
[56] Ping-Hung Yuh, Chia-Lin Yang, Yao-Wen Chang, BioRoute: a network-flow-based routing algorithm for the synthesis of digital microfluidic biochips, IEEE Trans. CAD Integr. Circuits Syst. 27 (11) (2008) 1928–1941.
[57] Tsung-Wei Huang, Tsung-Yi Ho, A fast routability- and performance-driven droplet routing algorithm for digital microfluidic biochips, in: ICCD, 2009, pp. 445–450.
[58] Pranab Roy, Hafizur Rahaman, Parthasarathi Dasgupta, A novel droplet routing algorithm for digital microfluidic biochips, in: ACM Great Lakes Symposium on VLSI, 2010, pp. 441–446.
[59] Oliver Keszöcze, Robert Wille, Krishnendu Chakrabarty, Rolf Drechsler, A general and exact routing methodology for digital microfluidic biochips, in: ICCAD, 2015, pp. 874–881.
[60] Tsung-Wei Huang, Chun-Hsien Lin, Tsung-Yi Ho, A contamination aware droplet routing algorithm for the synthesis of digital microfluidic biochips, IEEE Trans. CAD Integr. Circuits Syst. 29 (11) (2010) 1682–1695.
[61] Yang Zhao, Krishnendu Chakrabarty, Cross-contamination avoidance for droplet routing in digital microfluidic biochips, IEEE Trans. CAD Integr. Circuits Syst. 31 (6) (2012) 817–830.
[62] Hailong Yao, Qin Wang, Yiren Shen, Tsung-Yi Ho, Yici Cai, Integrated functional and washing routing optimization for cross-contamination removal in digital microfluidic biochips, IEEE Trans. CAD Integr. Circuits Syst. 35 (8) (2016) 1283–1296.
[63] Zipeng Li, Kelvin Yi-Tse Lai, Po-Hsien Yu, Tsung-Yi Ho, Krishnendu Chakrabarty, Chen-Yi Lee, High-level synthesis for micro-electrode-dot-array digital microfluidic biochips, in: DAC, 2016, pp. 146:1–146:6.
[64] Daniel T. Grissom, Philip Brisk, Fast online synthesis of digital microfluidic biochips, IEEE Trans. CAD Integr. Circuits Syst. 33 (3) (2014) 356–369.
[65] Advanced Circuits. http://www.4pcb.com.
[66] Mohamed Ibrahim, Krishnendu Chakrabarty, Efficient error recovery in cyberphysical digital-microfluidic biochips, IEEE Trans. Multi-Scale Comput. Syst. 1 (1) (2015) 46–58.
[67] Arash Abadian, Shahin Jafarabadi-Ashtiani, Paper-based digital microfluidics, Microfluid. Nanofluidics 16 (5) (2014) 989–995.
[68] Hyojin Ko, Jumi Lee, Yongjun Kim, Byeongno Lee, Chan-Hee Jung, Jae-Hak Choi, Oh-Sun Kwon, Kwanwoo Shin, Active digital microfluidic paper chips with inkjet patterned electrodes, Adv. Mater. 26 (15) (2014) 2335–2340.
[69] Ryan Fobel, Andrea E. Kirby, Alphonsus H.C. Ng, Ramin R. Farnood, Aaron Wheeler, Paper microfluidics goes digital, Adv. Mater. 26 (18) (2014) 2838–2843.
[70] Rüdiger Trojok, Alessandro Volpato, Mirela Alistar, Jorma Schubert, Auryn: Adaptor for General-purpose Digital Microfluidic Biochips, Zenodo, 2016.
[71] Ryan Fobel, Christian Fobel, Aaron R. Wheeler, DropBot: an open-source digital microfluidic control system with precise control of electrostatic driving force and instantaneous drop velocity measurement, Appl. Phys. Lett. 102 (2013), 193513.